

PAPER

Formation of Mn_5Ge_3 by thermal annealing of evaporated Mn on doped Ge on Si(111)

To cite this article: Stefan Bechler *et al* 2018 *Semicond. Sci. Technol.* **33** 095008

View the [article online](#) for updates and enhancements.






IOP | ebooks™

Bringing you innovative digital publishing with leading voices
to create your essential collection of books in STEM research.

Start exploring the **collection** - download the first chapter of
every title for free.

Formation of Mn_5Ge_3 by thermal annealing of evaporated Mn on doped Ge on Si(111)

Stefan Bechler¹ , Michal Kern², Hannes Simon Funk¹, Gerard Colston³, Inga Anita Fischer¹, David Weißhaupt¹, Maksym Myronov³ , Joris van Slageren²  and Jörg Schulze¹

¹Institute for Semiconductor Engineering and Center for Integrated Quantum Science and Technology, Universität Stuttgart, Pfaffenwaldring 47, Stuttgart, D-70569, Germany

²Institute of Physical Chemistry and Center for Integrated Quantum Science and Technology, Universität Stuttgart, Pfaffenwaldring 55, Stuttgart, D-70569, Germany

³Department of Physics, University of Warwick, Coventry CV4 7AL, United Kingdom

Received 31 March 2018, revised 4 July 2018

Accepted for publication 20 July 2018

Published 3 August 2018



Abstract

Mn_5Ge_3 can be used as a ferromagnetic contact material to fabricate spintronic devices. Here, we show that Mn_5Ge_3 can be fabricated with a simple germanidation process by evaporating Mn on undoped and doped Ge on Si followed by a thermal annealing step to form the ferromagnetic Mn_5Ge_3 phase. This solid phase preparation of Mn_5Ge_3 is a robust process with a minor dependence on the annealing parameters. The formation of Mn_5Ge_3 can be realized using undoped as well as highly doped p-Ge and n-Ge with different doping levels. The interface of Mn_5Ge_3 is atomically sharp which leads to very low contact resistivities $< 1 \times 10^{-7} \Omega \text{ cm}^2$.

Keywords: germanium, spintronics, spin injection, germanidation, Mn_5Ge_3 , thermal annealing

(Some figures may appear in colour only in the online journal)

1. Introduction

Spintronic devices, in which electron spin is used in addition to or instead of electron charge for logic devices, are promising candidates for beyond complementary metal–oxide–semiconductor (CMOS) concepts. For many of the device concepts such as spin-FETs [1] or all spin logic devices [2], the optimization of spin injection into a semiconductor channel, spin transport, spin manipulation in the channel and spin detection are key challenges. The injection of spin-polarized electrons into a semiconductor channel can be accomplished by using ferromagnetic electrodes with or without a tunneling barrier. Ideally, the ferromagnetic electrode material is chosen such that a highly spin-polarized current in the semiconductor as well as low specific contact resistivities can be realized. While large spin polarizations have been achieved using Fe/MgO tunneling contacts [3], the specific contact resistivities obtained with tunneling contacts are orders of magnitude higher (e.g. $1.5 \times 10^{-2} \Omega \text{ cm}^2$ for CoFeB/MgO/n⁺-Ge [4]) than the requirements for scaled-down devices ($< 10^{-8} \Omega \text{ cm}^2$) [5]. Furthermore, the fabrication process is difficult to integrate into a CMOS process. Mn_5Ge_3 has recently come into focus as ferromagnetic

contact material for spin injection into Ge [6, 7]. Its high Curie temperature of 296 K (which can be extended up to 450 K by adding C [8]), as well as its large degree of spin polarization (42%) [9] make it suitable as a ferromagnetic electrode material. Importantly, its conductivity is comparable to that of highly doped Ge, so that there is no need to introduce a tunneling or Schottky barrier to prevent conductivity mismatch [10]. Various methods have been used to fabricate $\text{Mn}_5\text{Ge}_3\text{C}_x$ and Mn_5Ge_3 layers. Those include the deposition of $\text{Mn}_5\text{Ge}_3\text{C}_x$ layers by simultaneous dc- and rf-magnetron sputtering from elemental targets of Mn, Ge and C in a high-vacuum system under Ar atmosphere at substrate temperatures $T_s = 400^\circ\text{C}$ – 500°C [11], the e-beam evaporation of Mn on Ge followed by an *in situ* annealing step at 350°C – 550°C [12], the successive e-beam evaporation of amorphous Ge and polycrystalline Mn films on $\text{SiO}_2/\text{Si}(100)$ substrates followed by *ex situ* annealing in an XRD setup [13], the Mn deposition or co-deposition of Mn and C from effusion cells on Ge(111) substrates in a molecular beam epitaxy (MBE) setup at room temperature followed by an *in situ* thermal annealing step at temperature of $\sim 450^\circ\text{C}$ [8], the successive thermal deposition of Mn and Ge layers on glass substrates at elevated substrate temperatures followed

Table 1. Sample series A. Annealing parameter for Al(80 nm)/Mn(18 nm)/i-Ge layer stack.

Sample		i-Ge 260slow	i-Ge 280slow	i-Ge 300slow	i-Ge 260fast	i-Ge 280fast	i-Ge 300fast
Start	(°C)	100	100	100	100	100	100
Ramp	(K min ⁻¹)	5	5	5	160	180	200
End	(°C)	260	280	300	260	280	300
Plateau	(min)	—	—	—	1	1	1
Ramp-down time	(min)	3	3	3	3	3	3

by an *in situ* annealing step [14, 15], and the co-deposition of Ge, Mn, and C at room temperature in a MBE setup on Ge buffer layers [16]. Here, we investigate another means of fabricating Mn₅Ge₃ layers, which is more closely related to industrially used silicide processes for contact formation. Mn films are deposited onto crystalline Ge surfaces by means of thermal evaporation and subjected to an *ex situ* annealing step in a rapid thermal processing (RTP) system. In this work we show that it is possible to fabricate Mn₅Ge₃ on undoped as well as p-type and n-type doped Ge(111) with a simple *ex situ* thermal annealing step of evaporated Mn on Ge. We discuss experimental measurements of the magnetic moment and of the specific contact resistivities in order to assess the potential of such contacts for spintronics applications.

2. Experimental

Three series of samples were fabricated in order to investigate (i) the influence of annealing parameters on the ferromagnetic properties of Mn₅Ge₃ (series A), (ii) the influence of Ge doping on the ferromagnetic properties of Mn₅Ge₃ (series B) and (iii) the specific contact resistivities of Mn₅Ge₃ formed on doped Ge samples (series C). An overview of the sample series A is given in table 1, overviews of sample series B and C are given in table 3.

The samples were fabricated starting with the growth of Ge on p⁻-Si(111) wafers using molecular beam epitaxy. After the growth of a 50 nm Si-buffer and 100 nm of Ge at a substrate temperature of 330 °C, the samples were annealed at 820 °C to form a Ge-virtual substrate (for details on the formation of thin virtual substrates we refer to [17]). This was followed by the growth of 300 nm of undoped Ge and 100 nm of doped Ge with varying dopant concentrations using B and Sb as dopant materials.

For all samples, Mn₅Ge₃ was formed as follows: the deposition of the Mn was carried out using thermal evaporation from a W boat at room temperature followed by the deposition of 30–80 nm of Al to prevent Mn from oxidizing. Before deposition of the metals, the samples were dipped in buffered HF for 10 s and rinsed in DI-water to clean the Ge surface and remove the native Ge oxide. Samples were then subjected to an *ex situ* thermal annealing step under N₂ atmosphere in an RTP system.

For series A and series B, the deposition of Mn and formation of Mn₅Ge₃ were investigated on unstructured samples. For series A with 7 samples, the annealing parameters (temperature ramp and maximum annealing

temperature) of the Al(80 nm)/Mn(18 nm)/Ge stack were varied as shown in table 1.

The maximum annealing temperature of 300 °C was selected to ensure sole growth of the Mn₅Ge₃ phase. Temperatures exceeding 300 °C were shown to grow the anti-ferromagnetic Mn₁₁Ge₈ phase which does not possess the desired magnetic properties [13].

In order to investigate the influence of doping on the formation of Mn₅Ge₃ (sample series B), the layer stacks of Al(65 nm)/Mn(20 nm)/Ge with different Sb ($1 \times 10^{18} \text{ cm}^{-3}$, $1 \times 10^{20} \text{ cm}^{-3}$) and B ($1 \times 10^{19} \text{ cm}^{-3}$, $1 \times 10^{20} \text{ cm}^{-3}$) doping levels were annealed with a ramp start temperature of 100 °C, a ramp end temperature of 300 °C and an average ramp up rate of 5 K min⁻¹. Annealing was done in a Seag-ASH SHS 200 RTP system. The ramp up was specifically designed to avoid overshoot of the ramp end temperature. Cooldown was achieved by increasing the N₂ flowrate, achieving a quasi-linear cooldown to a temperature of 150 °C at a rate of 80 K min⁻¹. After processing, the samples of series A and B were diced into $3 \times 3 \text{ mm}^2$ pieces and characterized using a superconducting quantum interference device (SQUID) magnetometer Quantum Design MPMS3. The measurements were performed in the maximum field range of -7 to +7 T allowed by the instrument to saturate the magnetic moment of the ferromagnetic Mn₅Ge₃. Before annealing, the samples of series A show a linear paramagnetic behavior. For all the annealed samples of series A and B, in order to see only the signal of the ferromagnetic layer, we therefore remove the linear paramagnetic background. For purpose of clarity the measurements are only shown from -1 to 1 T. High resolution transmission electron microscopy (HRTEM) was carried out to assess the crystal structure of the heterostructure. Measurements were performed using a JEOL 2100 TEM operating at an accelerating voltage of 200 kV. Sample cross sections were prepared through mechanical grinding and Ar milling within a precision ion polishing system to achieve electron transparency.

Finally, the formation of Mn₅Ge₃ was incorporated into a device fabrication process in series C in order to obtain transfer length measurement (TLM) structures for the measurement of the specific contact resistivities. Here, device fabrication started with the structuring of a mesa using photolithography and reactive ion etching. SiO₂ was then deposited as a passivation layer in a plasma-enhanced chemical vapor deposition system. After opening of contact holes using photolithography and reactive ion etching, the contact metals Mn and Al were deposited and structured with a lift-off process. The resistivity of the doped Ge layers and the

contact resistivity of the $\text{Mn}_5\text{Ge}_3/\text{Ge}$ interface were extracted from TLM measurements (details on the TLM structures and the measurement can be found in [11]).

3. Dependence of the formation of Mn_5Ge_3 on the annealing parameters

In sample series A we investigated the dependence of the formation of Mn_5Ge_3 on the annealing parameters. The samples differ in the maximum annealing temperature and the ramp up rate to reach the end temperature according to table 1. The temperature profile of the rapid thermal annealing process of the samples i-Ge260/280/300fast is shown in figure 1.

Before presenting the results of the magnetic moment measurements for series A, we discuss the formation and crystal quality of Mn_5Ge_3 by analyzing low and high resolution TEM images obtained from the i-Ge300fast sample. Figure 2 shows a low resolution TEM of the sample i-Ge300fast. Both bright field (BF) and dark field (DF) images are shown, taken in the (111) diffraction condition. On top of the MBE grown Ge layer, three different layers can be seen. Those are the Mn_5Ge_3 , the remaining Mn that was not consumed in the formation of Mn_5Ge_3 , and the Al cap layer. The thickness of the Mn_5Ge_3 layer is ~ 12 nm and the thickness of the remaining Mn is ~ 10 nm. The original Mn thickness was 18 nm, indicating that a Mn film with a thickness of 8 nm contributed to the formation of the 12 nm thick Mn_5Ge_3 layer. The dark field image shows only a low intensity for the Mn_5Ge_3 and no intensity for the Mn and Al, indicating that the Mn_5Ge_3 is not single crystalline but is most likely polycrystalline.

The higher magnification TEM images in figure 3 show the lattice planes of both the diamond cubic Ge, as well as the hexagonal Mn_5Ge_3 can be seen. Importantly, the diffusion process of the Mn and Ge results in an atomically flat interface between Ge and Mn_5Ge_3 . Due to the symmetry of the Ge(111) surface and the hexagonal Mn_5Ge_3 lattice, the Mn_5Ge_3 crystal is oriented with the c -axis perpendicular to the Ge(111) surface. No formation of Mn_xGe_y clusters in the Ge layer, which was observed in previous investigations [18], can be seen in our samples. In our samples, the Mn is not fully consumed in the Mn_5Ge_3 formation process and the remaining Mn forms an amorphous layer between the Mn_5Ge_3 and the Al cap layer. The atomically flat interface between Mn_5Ge_3 and the Ge channel and the good crystallinity of the Mn_5Ge_3 hexagonal lattice are expected to be beneficial for spin injection. In contrast to the atomically flat interface between the Ge and the Mn_5Ge_3 , the interface between Mn_5Ge_3 and the residual Mn is not very well defined, leading to a significant variation of the thickness of the formed Mn_5Ge_3 over the sample.

In order to characterize the interface between Mn_5Ge_3 and the residual Mn, the sample i-Ge 300fast was etched in phosphoric acid ($C = 184 \text{ mol l}^{-1}$) for 1 min to remove the Al and the Mn. Figure 3(a) shows the SEM image of this etched sample, figures 4(b) and (c) the AFM image and the

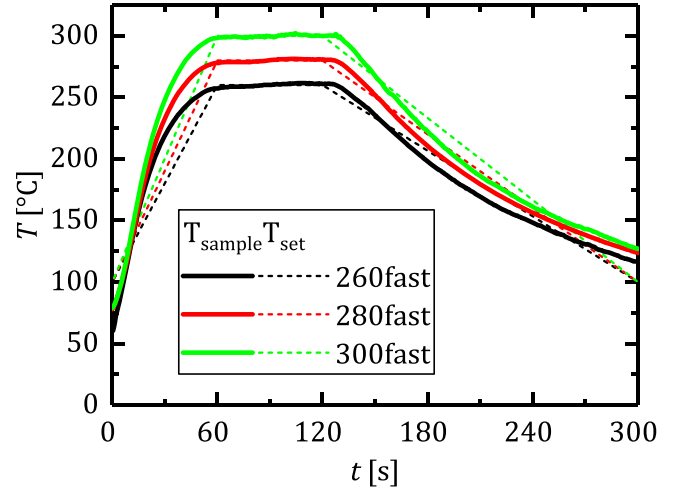


Figure 1. Temperature profile of the rapid thermal annealing process.

profile along the A–A' plane. The uneven surface with a surface roughness $\text{rms} = 2.25$ nm can be a result of inhomogeneous Mn_5Ge_3 etching. However, given the uneven interface between the Mn_5Ge_3 and the remaining Mn that can be seen already in the cross sectional TEM image, the roughness can also originate from inhomogeneous Mn_5Ge_3 formation on the sample. One possible strategy to improve interface quality is to reduce the thickness of the Mn layer such that no Mn remains after the formation of the Mn_5Ge_3 layer.

Figure 5 shows the temperature dependence of the magnetic moment for samples of series A. The measurement is performed at an in-plane magnetic field of $\mu_0 H = 0.1$ T. All samples have a Curie temperature of ~ 300 K showing that for all the samples the ferromagnetic phase Mn_5Ge_3 is formed and no other phase is dominant.

Figure 6(a) shows the magnetic moment at 5 K of the sample i-Ge 300fast. Clear ferromagnetic behavior can be observed with a preferred in-plane magnetization and a non-negligible out-of-plane magnetization. Extracting coercivity ($\mu H_c = 65$ mT) and remanence ($m_{\text{rem}}/m_{\text{Sat}} = 45\%$) from the hysteresis curve and comparing it with [8, 19], we can estimate the thickness of the formed Mn_5Ge_3 to be $d \sim 16$ nm, which is close to the value extracted from the TEM images. Again, this confirms that not all of the Mn is consumed to form the Mn_5Ge_3 . As discussed in detail in [19], depending on the thickness of the Mn_5Ge_3 layer the magnetization easy axis rotates from in-plane for thicknesses < 10 nm to out-of-plane for film thicknesses > 20 nm: for film thicknesses < 10 nm, a monodomain-type structure is formed, while for film thicknesses between 10 and 20 nm, a continuous reorientation of the magnetization from in-plane to out-of-plane has been observed.

The in-plane hysteresis curves at 5 K of all samples of series A are shown in figure 6(b). All samples show a similar ferromagnetic behavior. The parameters saturation magnetic moment m_{Sat} , remanence m_{Rem} , and coercivity μH_c were extracted for all samples and are shown in table 2. There is a

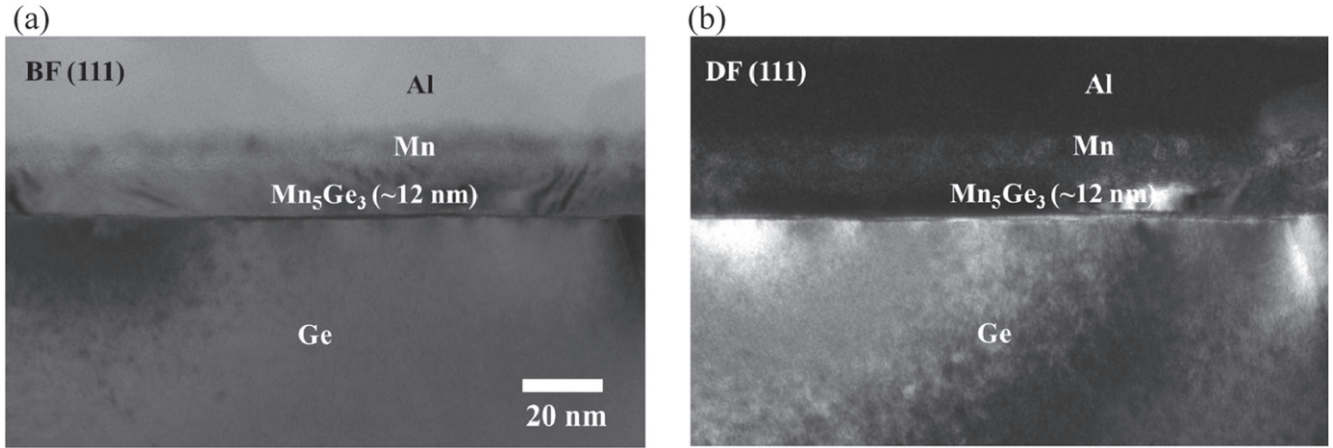


Figure 2. Cross sectional TEM imaged of the Al/Mn(10 nm)/Mn₅Ge₃(12 nm)/i-Ge layer stack taken in BF (a) and DF (b) diffraction conditions. The thickness of the Mn before annealing was 18 nm.

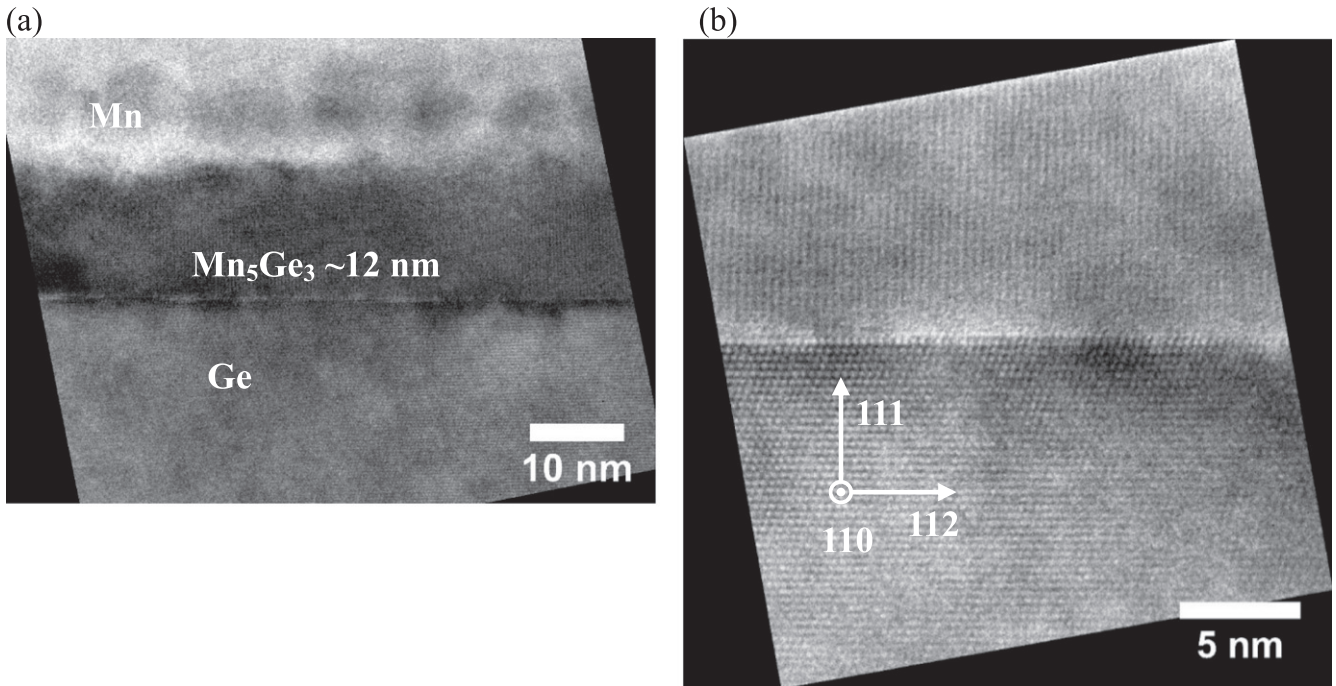


Figure 3. (a) HRTEM image of the Al/Mn(10 nm)/Mn₅Ge₃(12 nm)/i-Ge/Si(111) layer stack and (b) HRTEM image with a higher resolution.

noticeable trend towards higher saturation of the magnetic moment with higher maximum annealing temperature. Furthermore, the ratio $m_{\text{Rem}}/m_{\text{Sat}}$ decreases as the maximum annealing temperature is increased and is lower for samples for which a fast ramp is applied for annealing compared to samples with slow ramps. The ratio $m_{\text{Rem}}/m_{\text{Sat}}$ has been shown to be a function of the thickness of the Mn₅Ge₃ layer [19] and to decrease monotonously with increasing layer thickness. Again comparing the values for $m_{\text{Rem}}/m_{\text{Sat}}$ extracted in our experiment to the data found in [19], we can estimate the thicknesses of our Mn₅Ge₃ layers to vary between 15 and 20 nm for all samples. This is in agreement with the HRTEM analysis. Our results also indicate that

within the range of annealing parameters investigated here, an increase in maximum annealing temperatures leads to an increase in Mn₅Ge₃ layer thickness. Moreover, faster temperature ramps at a fixed maximum annealing temperature lead to a reduction in Mn₅Ge₃ layer thickness. A likely explanation for these trends is that slower temperature ramps and higher maximum annealing temperatures both enhance material interdiffusion and, thus, lead to an increase in Mn₅Ge₃ layer thickness. Nonetheless, we find that the formation of Mn₅Ge₃ by annealing is a fast and robust process that does not show a strong dependence on the thermal budget spent to form the Mn₅Ge₃ layer within the parameter range investigated here. Low annealing temperatures are beneficial to

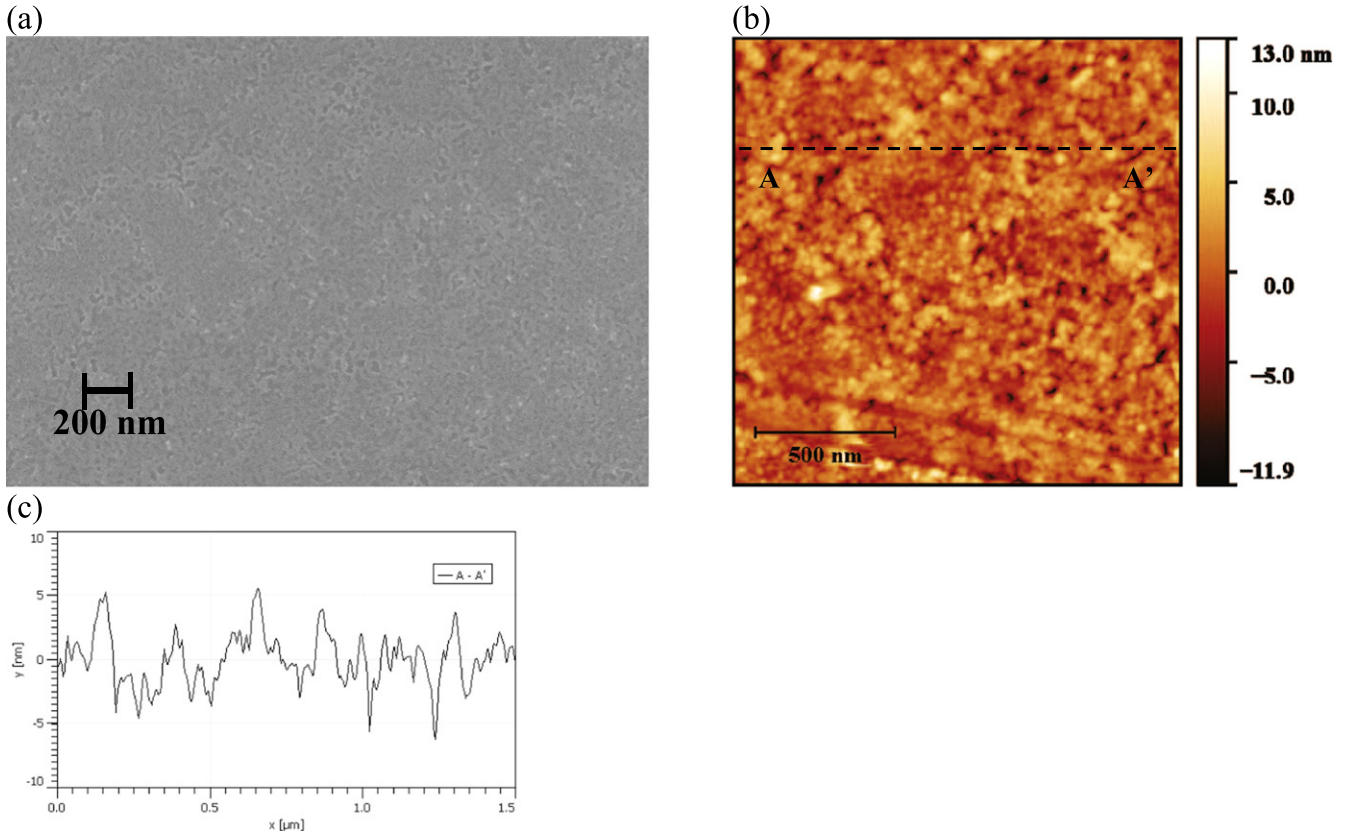


Figure 4. (a) SEM image of the sample iGe300slow after removal of Al and residual Mn using phosphoric acid. (b) AFM image of the sample iGe300slow. (c) Profile along A–A'.

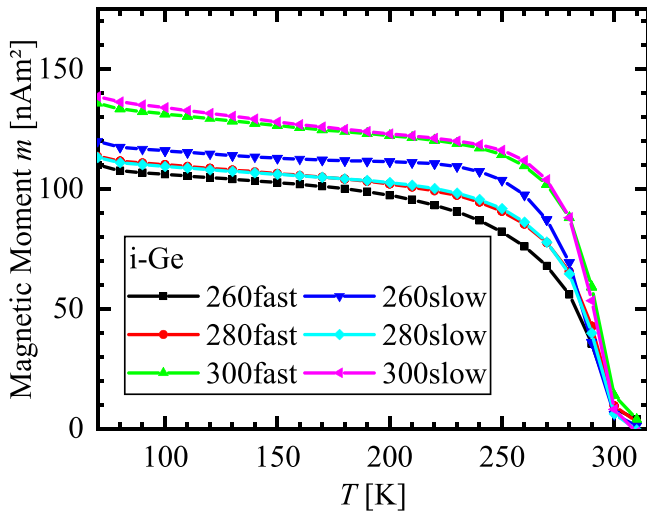


Figure 5. Temperature dependence of the in-plane magnetic moment for sample series A.

reduce the thermal budget for device processing and avoid dopant out-diffusion in the semiconductor layers. Therefore we did not extend the annealing temperature range in contrast to previously reported work (e.g. Nishimura *et al* used annealing temperatures between 350 °C and 500 °C [12]), which can explain why the thickness of our Mn_5Ge_3 layers is limited. Finally, limiting the thickness of ferromagnetic Mn_5Ge_3 electrodes on Ge(111) for spin injection to below

10 nm is crucial in order to constrain the easy axis to an in-plane direction. In our setup, this can be achieved by further reducing the annealing temperature or by limiting the thickness of the deposited Mn.

4. Dependence of the formation of Mn_5Ge_3 on the doping of the Ge

For development of spintronic devices, it is important to investigate the formation of Mn_5Ge_3 for undoped as well as for p-doped and n-doped Ge. This investigation was carried out using sample series B and C.

Figures 7(a) and (b) show the magnetic hysteresis curves recorded on the samples of series B for in-plane and out-of-plane orientations. The samples show a clear ferromagnetic behavior with a preferred in-plane magnetization but a sizeable out-of-plane magnetization. Comparing the magnetic moment for the different doping levels, there are only minor differences in the saturation magnetic moment and only the sample n-Ge1e18 shows a different shape of the hysteresis for in-plane as well as out-of-plane magnetic field that will be discussed below. No obvious correlation of the saturation magnetic moment to the doping type and doping level can be found. The difference in the saturation magnetic moment can be attributed to small differences in the thickness of the formed Mn_5Ge_3 and differences in sample area. From the similarity of the out-of-plane hysteresis curves, we conclude

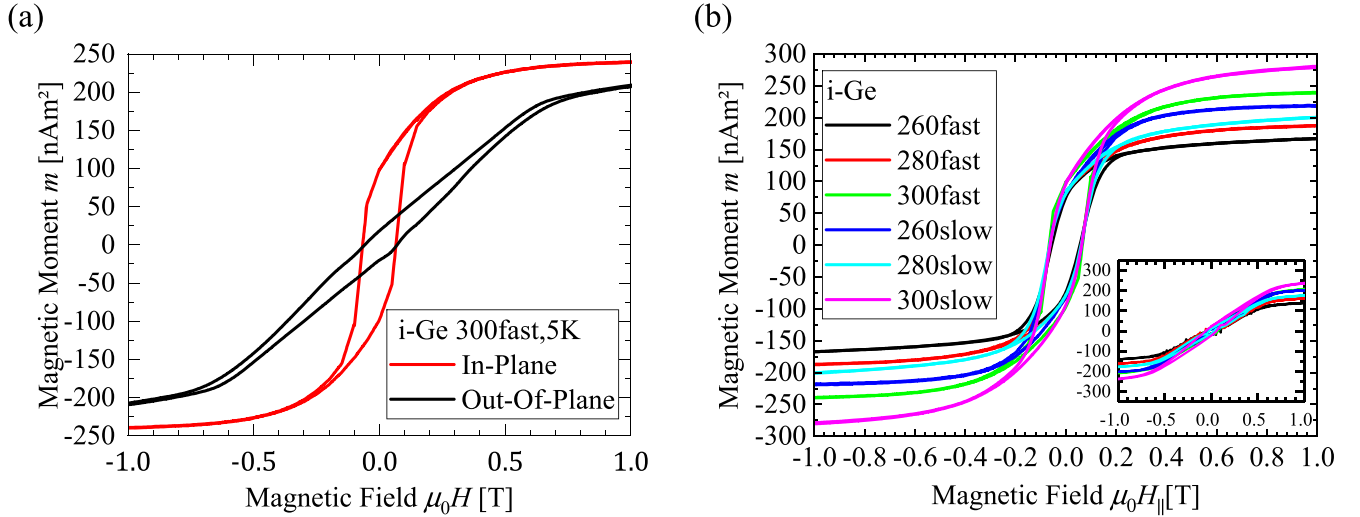


Figure 6. (a) In-plane and out-of-plane hysteresis of sample i-Ge300fast. (b) In-plane hysteresis of the samples of series A with a layer stack of Al(80 nm)/Mn(18 nm)/i-Ge at 5 K. Inset: out-of-plane hysteresis of the samples of series A at 5 K.

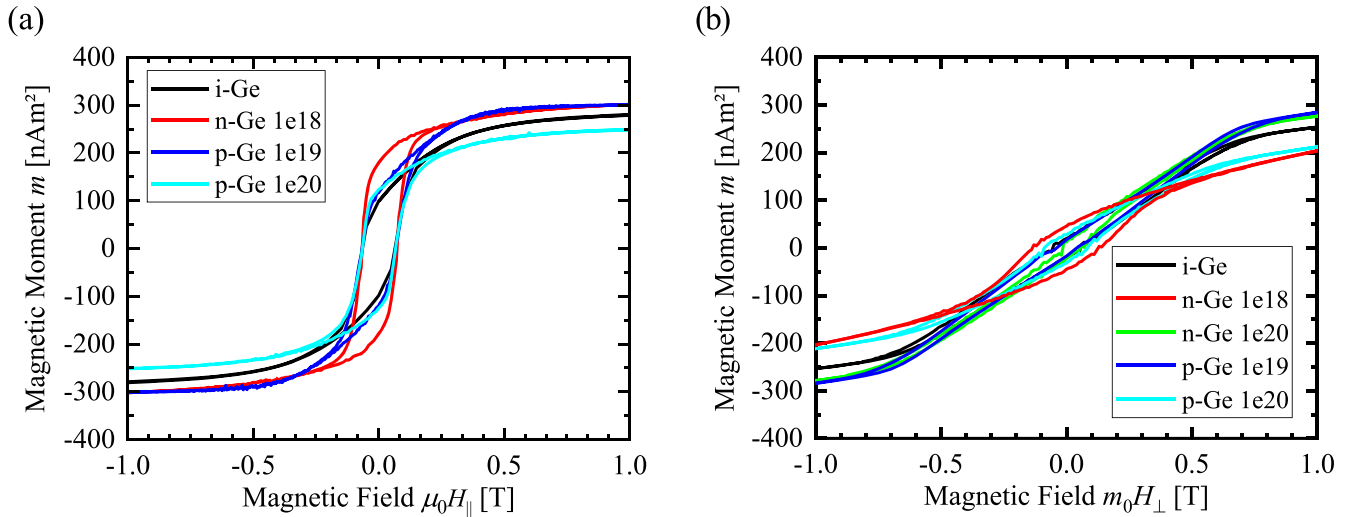


Figure 7. (a) In-plane hysteresis of the samples of series B with a layer stack of Al(65 nm)/Mn(20 nm)/Ge at 5 K. (b) Out-of-plane hysteresis of the samples of series B at 5 K.

Table 2. Summary of the extracted parameters from the SQUID measurement for sample series A.

Sample	i-Ge 260fast	i-Ge 280fast	i-Ge 300fast	i-Ge 260slow	i-Ge 280slow	i-Ge 300slow
m_{Rem} (nA m ²)	82	83	98	83	84	99
m_{Sat} (nA m ²)	162	206	249	222	222	301
$m_{\text{Rem}}/m_{\text{Sat}}$	0.50	0.40	0.39	0.37	0.37	0.33
$\mu_0 H_{\text{coer}}$ (T)	0.057	0.063	0.066	0.064	0.065	0.062

that even the high doping levels of $1 \times 10^{20} \text{ cm}^{-3}$ for both Sb and B doped Ge do not strongly affect or even hinder the formation of Mn_5Ge_3 . Thus, with our Mn_5Ge_3 fabrication process it is possible to realize a ferromagnet with a germanide process even on doped Ge that is similar to the well known silicidation process and can potentially be part of a CMOS compatible device fabrication process.

Since the hysteresis loop of n-Ge1e18 is qualitatively slightly different from the other samples of series B, we discuss this sample in more detail. Compared to sample n-Ge1e20, the lower dopant concentration of sample n-Ge18 was obtained by increasing the substrate temperature during growth to 330 °C rather than reducing the Sb flux. It is well known that segregation of Sb in Ge is strongly influenced by

Table 3. Sample series B and C. The Al(65 nm)/Mn(20nm)/Ge layer stacks were annealed starting at 100 °C with a maximum annealing temperature of 300 °C and a 5 K min⁻¹ ramp. The specific contact resistivity and sheet resistance were extracted from TLM measurements.

Sample		i-Ge	n-Ge1e18	n-Ge1e20	p-Ge1e20	p-Ge1e19
Thickness Ge	(nm)	100	100	100	100	100
Growth temperature	(°C)	330	330	160	330	330
Doping	(cm ⁻³)	—	1×10^{18}	1×10^{20}	1×10^{20}	1×10^{19}
ρ_c	(Ω cm ²)	—	$1.3 \times 10^{-6} \pm 1.6 \times 10^{-7}$	$7.2 \times 10^{-7} \pm 1.9 \times 10^{-7}$	$1.6 \times 10^{-8} \pm 1.8 \times 10^{-8}$	$1.8 \times 10^{-6} \pm 5.3 \times 10^{-7}$
R_{sh}	(Ω /sq)	—	459 ± 18	48 ± 0.87	100 ± 0.15	144 ± 2.1
ρ_{Ge}	(Ω cm)	—	4.59×10^{-3}	3.10×10^{-4}	1.00×10^{-3}	1.45×10^{-3}

substrate temperature [20]. However, as a consequence segregated Sb remains on the surface of the Ge and can influence the Mn_5Ge_3 formation. The strong rectangular hysteresis of the in-plane magnetization with $m_{\text{rem}}/m_{\text{Sat}} = 57\%$ indicates that the Mn_5Ge_3 layer has a thickness of ~ 10 nm, i.e. the out-of-plane magnetization should be negligible [8, 19]. This, however, is not borne out by our experimental results: we see a remarkably wide open hysteresis for the out-of-plane magnetization with a higher coercivity compared to the coercivity for in-plane magnetization. The explanation of this observation is currently not clear to us.

Finally, we note that the extracted specific contact resistivities of the sample of series C (see table 3) are very low $< 1.7 \times 10^{-6} \Omega \text{ cm}^2$ for p-type as well as n-type doping. Importantly, these values are significantly lower than the specific contact resistivities typically found for ferromagnetic tunnel contacts (e.g. $1.5 \times 10^{-2} \Omega \text{ cm}^2$ for $\text{CoFeB}/\text{MgO}/\text{n}^+\text{-Ge}$ [4]). This demonstrates that Mn_5Ge_3 as a ferromagnetic contact material with small specific contact resistivities is particularly interesting for scaled-down devices.

5. Conclusion

In this work we show that a germanidation process by rapid thermal annealing of thermally evaporated Mn on undoped and doped Ge layers on Si wafers leads to the formation of ferromagnetic Mn_5Ge_3 with a preferred in-plane magnetization and a layer thickness of $\sim 15\text{--}20$ nm. High resolution TEM images reveal a high quality $\text{Mn}_5\text{Ge}_3/\text{Ge}$ interface, which is expected to be beneficial for spin injection into Ge. We find that the doping of the Ge layers has no strong influence on the magnetic properties of the Mn_5Ge_3 layers. Furthermore, specific contact resistivities for Mn_5Ge_3 on highly doped p-Ge as well as n-Ge are low ($< 1.7 \times 10^{-6} \Omega \text{ cm}$). Our investigation is an important step towards the fabrication of spintronic devices, in which the ferromagnetic contacts are fabricated in a CMOS compatible process. Future experiments will investigate spin injection into doped Ge channels based on the ferromagnetic contact formation process developed here.

Acknowledgments

This work was funded by the Center for Integrated Quantum Science and Technology IQST and by the DFG under Grant FI 1511/3-1.

ORCID iDs

Stefan Bechler  <https://orcid.org/0000-0002-4887-2743>

Maksym Myronov  <https://orcid.org/0000-0001-7757-2187>

Joris van Slageren  <https://orcid.org/0000-0002-0855-8960>

References

- [1] Sugahara S and Tanaka M 2004 A spin metal–oxide–semiconductor field-effect transistor using half-metallic-ferromagnet contacts for the source and drain *Appl. Phys. Lett.* **84** 2307
- [2] Behin-Aein B, Datta D, Salahuddin S and Datta S 2010 Proposal for an all-spin logic device with built-in memory *Nat. Nanotechnol.* **5** 266–70
- [3] Spiesser A, Saito H, Fujita Y, Yamada S, Hamaya K, Yuasa S and Jansen R 2017 Giant spin accumulation in silicon nonlocal spin-transport devices *Phys. Rev. Appl.* **8** 064023
- [4] Lee D, Raghunathan S, Wilson R J, Nikonov D E, Saraswat K and Wang S X 2010 The influence of Fermi level pinning/depinning on the Schottky barrier height and contact resistance in Ge/CoFeB and $\text{Ge}/\text{MgO}/\text{CoFeB}$ structures *Appl. Phys. Lett.* **96** 052514
- [5] Coss B E, Smith C, Loh W Y, Majhi P, Wallace R M, Kim J and Jammy R 2011 Contact resistance reduction to FinFET source/drain using novel dielectric dipole Schottky barrier height modulation method *IEEE Electron Device Lett.* **32** 862–4
- [6] Spiesser A, Saito H, Jansen R, Yuasa S and Ando K 2014 Large spin accumulation voltages in epitaxial Mn_5Ge_3 contacts on Ge without an oxide tunnel barrier *Phys. Rev. B* **90** 205213
- [7] Fischer I A, Chang L-T, Sürgers C, Rolseth E, Reiter S, Stefanov S, Chiussi S, Tang J, Wang K L and Schulze J 2014 Hanle-effect measurements of spin injection from $\text{Mn}_5\text{Ge}_3\text{C}_{0.8}/\text{Al}_2\text{O}_3$ -contacts into degenerately doped Ge channels on Si *Appl. Phys. Lett.* **105** 222408
- [8] Thanh V L, Spiesser A, Dau M-T, Olive-Mendez S F, Michez L A and Petit M 2013 Epitaxial growth and magnetic properties of $\text{Mn}_5\text{Ge}_3/\text{Ge}$ and $\text{Mn}_5\text{Ge}_3\text{C}_x/\text{Ge}$ heterostructures for spintronic applications *Adv. Nat. Sci.: Nanosci. Nanotechnol.* **4** 043002
- [9] Panguluri R P, Zeng C, Weitering H H, Sullivan J M, Erwin S C and Nadgorny B 2005 Spin polarization and electronic structure of ferromagnetic Mn_5Ge_3 epilayers *Phys. Status Solidi b* **242** R67–9
- [10] Schmidt G, Ferrand D, Molenkamp L W, Filip A T and van Wees B J 2000 Fundamental obstacle for electrical spin injection from a ferromagnetic metal into a diffusive semiconductor *Phys. Rev. B* **62** R4790
- [11] Fischer I A, Gebauer J, Rolseth E, Winkel P, Chang L-T, Wang K L, Sürgers C and Schulze J 2013 Ferromagnetic $\text{Mn}_5\text{Ge}_3\text{C}_{0.8}$ contacts on Ge: work function and specific contact resistivity *Semicond. Sci. Technol.* **28** 125002
- [12] Nishimura T, Nakatsuka O, Akimoto S, Takeuchi W and Zaima S 2011 Crystalline orientation dependence of electrical properties of Mn germanide/ $\text{Ge}(1\ 1\ 1)$ and $(0\ 0\ 1)$ Schottky contacts *Microelectron. Eng.* **88** 605–9
- [13] Abbas O, Portavoce A, Thanh V L, Girardeaux C and Michez L 2013 Phase formation during Mn thin film reaction with Ge: self-aligned germanide process for spintronics *Appl. Phys. Lett.* **103** 172405
- [14] Myagkov V G, Zhigalov V S, Matsynin A A, Bykova L E, Bondarenko G V, Bondarenko G N, Patrino G S and Velikanov D A 2012 Phase transformations in the Mn–Ge system and in $\text{Ge}_x\text{Mn}_{1-x}$ diluted semiconductors *JETP Lett.* **96** 40–3
- [15] Myagkov V G, Zhigalov V S, Matsynin A A, Bykova L E, Mikhlin Y L, Bondarenko G N, Patrino G S and Yurkin G Y 2014 Formation of ferromagnetic germanides by solid-state reactions in $20\text{Ge}/80\text{Mn}$ films *Thin Solid Films* **552** 86–91
- [16] Petit M, Michez L, Dutoit C-E, Bertina S, Dolocan V O, Heresanu V, Stoffel M and Le Thanh V 2015 Very low-

- temperature epitaxial growth of Mn_5Ge_3 and $\text{Mn}_5\text{Ge}_3\text{C}_{0.2}$ films on Ge(111) using molecular beam epitaxy *Thin Solid Films* **589** 427–32
- [17] Kasper E and Lyutovich K 2004 Strain adjustment with thin virtual substrates *Solid-State Electron.* **48** 1257–63
- [18] Spiesser A *et al* 2011 Control of magnetic properties of epitaxial $\text{Mn}_5\text{Ge}_3\text{C}_x$ films induced by carbon doping *Phys. Rev. B* **84** 165203
- [19] Michez L-A, Spiesser A, Petit M, Bertaina S, Jacquot J-F, Dufeu D, Coudreau C, Jamet M and Thanh V L 2015 Magnetic reversal in Mn_5Ge_3 thin films: an extensive study *J. Phys.: Condens. Matter* **27** 266001
- [20] Yurasov D V, Antonov A V, Drozdov M N, Schmagin V B, Spirin K E and Novikov A V 2015 Antimony segregation in Ge and formation of n-type selectively doped Ge films in molecular beam epitaxy *J. Appl. Phys.* **118** 145701